Climate-Driven Basin-Scale Decadal Oscillations of Oceanic Phytoplankton

Elodie Martinez, *et al.*

Science **326**, 1253 (2009);
DOI: 10.1126/science.1177012

Climate-Driven Basin-Scale Decadal Oscillations of Oceanic Phytoplankton

Elodie Martinez,* David Antoine, Fabrizio D'Ortenzio, Bernard Gentili

Phytoplankton—the microalgae that populate the upper lit layers of the ocean—fuel the oceanic food web and affect oceanic and atmospheric carbon dioxide levels through photosynthetic carbon fixation. Here, we show that multidecadal changes in global phytoplankton abundances are related to basin-scale oscillations of the physical ocean, specifically the Pacific Decadal Oscillation and the Atlantic Multidecadal Oscillation. This relationship is revealed in ~20 years of satellite observations of chlorophyll and sea surface temperature. Interaction between the main pycnocline and the upper ocean seasonal mixed layer is one mechanism behind this correlation. Our findings provide a context for the interpretation of contemporary changes in global phytoplankton and should improve predictions of their future evolution with climate change.

Knowledge of decadal-scale changes in the distribution and abundance of ocean phytoplankton at a global scale remains uncertain. These changes result from processes occurring at a variety of time scales, including (possibly) the centennial one of anthropogenic global warming, interdecadal ones at basin-to-global scales, and interannual to seasonal ones. Understanding how processes intermingled at these different scales modify phytoplankton distributions requires global, multidecadal time series of chlorophyll concentration (Chl). This concentration describes at first order changes in phytoplankton biomass and also reflects the photoacclimation state of phytoplankton; that is, the modification of intracellular Chl in response to the average light level in the upper layers of the ocean. The best available tool for a global description of Chl is the remote sensing of ocean color from satellites, which allows multiyear global time series to be built from repeated synoptic observations.

Existing ocean color archives are relatively short in duration, however, so the long-term trend that may result from anthropogenic warming is neither unambiguously identified nor quantified. Contradictory results have been published as to whether the global ocean biomass increased or decreased from the 1980s to the 2000s (*1*, *2*). On the other hand, interannual-to-seasonal time scales have been intensively investigated on scales ranging from regional to global (*3*–*5*), in particular thanks to the 10-year time series provided by the Sea-viewing Wide Field-of-view Sensor (SeaWiFS) (*6*).

We focused on the multidecadal scale, by using a consistent, reanalyzed (*1*), ocean color time series built from 5 years of observations of the Coastal Zone Color Scanner (CZCS; 1979–1983) (*7*, *8*) and 5 years from SeaWiFS (1998–2002) (fig. S1). In parallel, a record of sea surface temperature (SST) (*8*, *9*) encompassing the same time period was used as an indicator of ocean stratification. These data sets allow us to perform a global quantification of the covariability of Chl and SST over two decades. We first describe how the inverse relationship between Chl and SST variabilities previously identified at interannual time scales for the SeaWiFS era (*4*) is also found over the decadal scale, but that the spatial distribution in the sign of these changes at the decadal scale is approximately a mirror image of those found over the SeaWiFS record. Multivariate empirical orthogonal function analyses (MEOFs) (*8*) were then performed in order to investigate the spatial and temporal signals behind this relationship, highlighting the role of basin-scale climate oscillators. Finally, other parameters were examined in order to propose a mechanism by which these oscillations of the physical environment affect the phytoplankton distribution.

Decadal changes in Chl and SST from the 1980s to the 2000s are displayed in Fig. 1, A and B, respectively. These maps highlight broad areas where Chl and SST evolved inversely. For the eastern and equatorial regions of the Pacific, SST decreased on average by 0.3°C, whereas in the western subtropical and western equatorial region, SST increased on average by 0.5°C (Fig. 1B). Changes in Chl, although more patchy than the SST changes, are roughly in the opposite direction, with large increases in the equatorial region where SST decreased. SST increased moderately (~0.2°C) in the Atlantic Ocean north of 30°S, and areas of inverse Chl and SST changes are less extensive there than in the Pacific. In the Indian Ocean, the areas where Chl and SST evolved inversely are mostly shaped by the distribution of the SST change, because Chl essentially increased everywhere in this ocean. Parallel increases of Chl and SST are the most frequent case (61%) in the Indian Ocean. This weak Chl-SST inverse relationship was also reported over the SeaWiFS era (*4*).

A map of the areas where Chl and SST evolve either in parallel (dark blue and purple) or inversely (light blue and yellow) is displayed in Fig. 1C. Overall, the regions of opposite Chl and SST changes represent about 60% of the ocean area comprised between latitudes 50°S and 50°N. This Chl-SST inverse correspondence was previously identified by (*4*) between 1999 and 2004 (Fig. 1D, similar to their figure 3C). The spatial distribution of the sign of these changes, as obtained here over two decades, is, however, approximately a mirror image of those found by (*4*) on interannual time scales. This appears in the Pacific when comparing Fig. 1, C and D. This inverted time evolution also appears regionally in the North Atlantic and barely shows up in the Indian Ocean. Therefore, when data over 1979–2002 (Fig. 1, A to C) or 1999–2004 (Fig. 1D) are analyzed, opposite directions of changes for SST and Chl are revealed in many regions. A large-scale multidecadal signal clearly emerges from this analysis, which indicates that oceanographic phenomena acting at basin scale shape the global decadal-scale phytoplankton distribution in the ocean.

The spatial patterns of the SST changes in the Pacific Ocean (Fig. 1B) actually bear the footprint of the Pacific Decadal Oscillation (PDO) (*10*), which is a pattern of SST anomalies in the subtropical North and South Pacific that are out of phase with SST anomalies in the tropical Pacific. In the Atlantic (Fig. 1B), a similar correspondence is observed with the Atlantic Multidecadal Oscillation (AMO) (*11*), whose pattern reveals SST anomalies that are homogeneous over the whole North Atlantic, positive for the period considered here. Other indexes such as the North Atlantic Oscillation or the Multivariate ENSO Index do not exhibit such spatial patterns, and their typical scales of variations are <~10 years, which makes them inappropriate for the present multidecadal analysis.

MEOFs were carried out over the 1979–2002 time period separately for the three oceanic basins (*8*). The reason for not doing a global analysis is that the Pacific represents ~50% of the global ocean and has the strongest SST and Chl signals, which overwhelm a global analysis, effectively masking the specific responses of the other oceans (*8*).

The spatial patterns of Chl and SST changes revealed in Fig. 1, A and B, also appear in the Chl and SST spatial variability maps made from the most significant components of the multidecadal signal (fig. S2). The Chl-SST common time variability associated with these spatial patterns is displayed for the three oceans in Fig. 2. In the Pacific Ocean (Fig. 2A), the signal shifts from negative to positive from 1979–1983 to 1998–2002, in correspondence with a shift from a PDO warm phase at the beginning of the 1980s to a cool phase at the end of the 1990s (*12*). Correlation between the PC and the PDO is 0.66 and reaches 0.83 when a 3-month lag between both is applied. There was a shift back to a PDO warm phase in 2002, which also appears in the Chl-SST time signal otherwise obtained over the 1998–2005 time period (right side of Fig. 2A; for a similar MEOFs analysis using the standard SeaWiFS

UPMC University of Paris 06, UMR 7093, Laboratoire d'Océanographie de Villefranche (LOV), 06230 Villefranche-sur-Mer, France; and CNRS, UMR 7093, LOV, 06230 Villefranche-sur-Mer, France.

*To whom correspondence should be addressed. E-mail: martinez@obs-vlfr.fr

Chl product, see fig. S3). This succession of opposite phases of the decadal oscillation corresponds to the opposite patterns obtained for the 1979–2002 (Fig. 1C) and 1999–2004 (Fig. 1D) analyses, for areas presenting opposite Chl and SST trends in this ocean (see also figs. S2 and S3). In the Indian Ocean, the Chl-SST covarying time signal also shifts from negative to positive from the beginning of the 1980s to the beginning of the 2000s (Fig. 2B). This shift may be related to the PDO [correlation coefficient (r) = 0.6] through the connection between the Indian and the Pacific. In the Atlantic, the sign of the time signal reverses from negative to positive from 1979–1983 to 1998–2002 (Fig. 2C). This corresponds to a shift of the AMO index from a cool to a warm phase in the 1990s (r = 0.75). On the contrary, the AMO index remains on average positive over the 1998–2005 period (right side of Fig. 2C). There is no shift from one phase of the decadal cycle to another, which explains why the spatial patterns in the Atlantic differ between Fig. 1C (1979–2002) and Fig. 1D (1999–2004) without being opposite as they are in the Pacific, however.

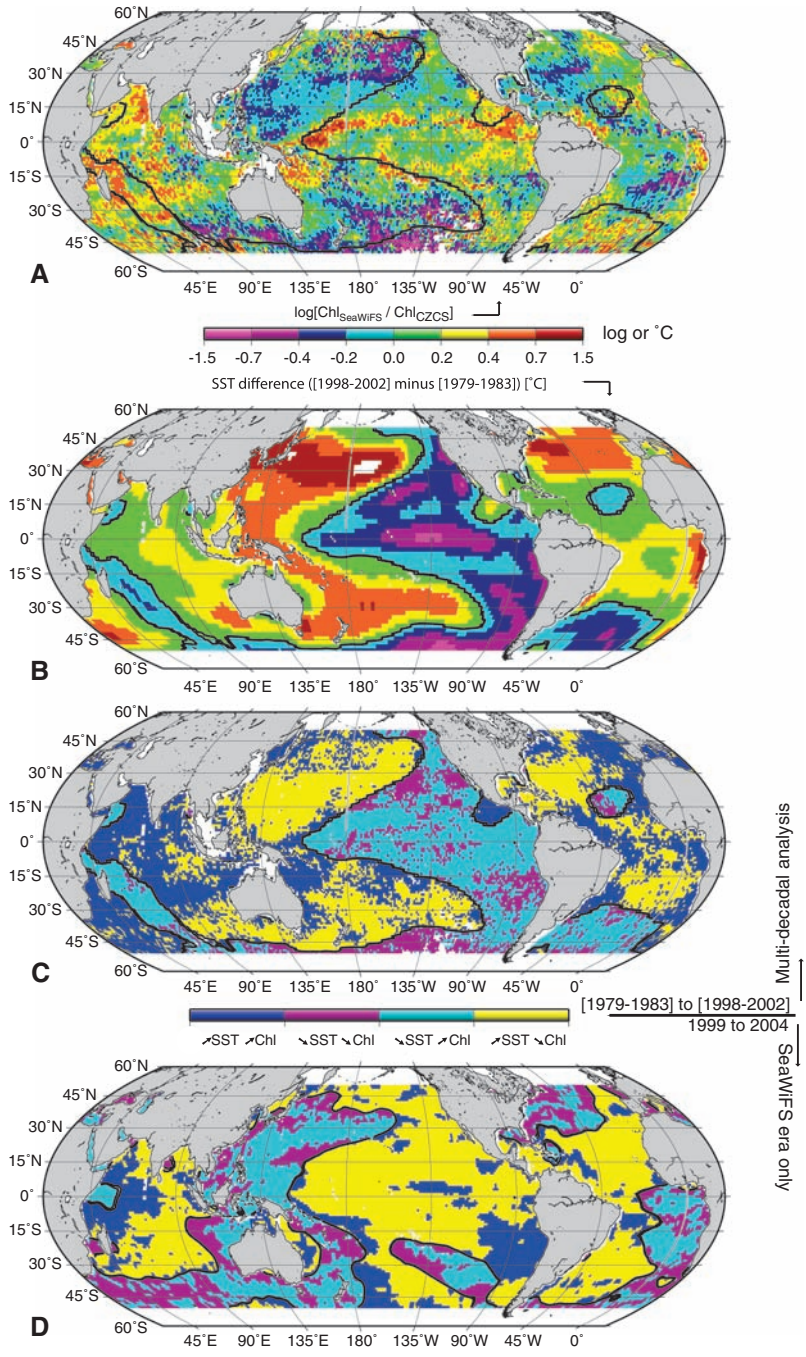

Fig. 1. (**A**) Chl change from the CZCS (1979–1983) to the SeaWiFS (1998–2002) era, expressed as the logarithm of the ratio of the average values over the two time periods [changes by a factor of 2 correspond to values of –0.7 (halving) or 0.7 (doubling)]. (**B**) SST difference over the same period. (**C**) Map of areas with concomitant parallel or opposite changes of Chl and SST, as indicated. (**D**) As in (C), but between 1999 and 2004, as in (*4*). The SST zero difference is shown on the maps as a thick black curve.

Correlations between basin-scale phytoplankton distribution and modes of climate oscillators are revealed here at multidecadal scale. In the tropics and at mid-latitudes, phytoplankton are often nutrient-limited. They grow when nutrients are made available within the upper lit layers through the upwelling of cold nutrient-rich water from below (or mixing with these deep waters). Therefore, any change of the overall stratification of the surface ocean has potential effects on phytoplankton growth, which may happen at different spatial and temporal scales. On seasonal-to-interannual time scales, there are changes of the depth of the upper ocean seasonal mixed layer (ZML). On decadal scales, the depth of the main pycnocline indicates the distance between the ZML (or the euphotic zone) and deep nutrient reservoirs. A proxy of the pycnocline is the depth of the 26 kg/m^3 isopycnal ($Z\rho_{26}$) (*13*), which is located between about 0 and 500 m within the intertropical area. Both ZML and $Z\rho_{26}$ were determined from the simple ocean data assimilation (SODA) model outputs (*8*, *14*).

The relationships between Chl and $Z\rho_{26}$ or ZML are displayed in Fig. 3 for the multidecadal analysis, similarly to the Chl-SST relationship shown in Fig. 1C. The patterns of $Z\rho_{26}$-Chl (Fig. 3A) and SST-Chl (Fig. 1C) show similarities, in particular in the Pacific and North Atlantic, showing that decadal-scale uplift or deepening of the pycnocline is the likely mechanism leading to the Chl-SST covariability. This inverse relationship is also found over almost the entire Indian Ocean. Changes in $Z\rho_{26}$ modify the average nutrient input to the upper lit layers, changing productivity and thereby chlorophyll levels. The geographical distribution of the Chl-ZML relationship (Fig. 3B) is not similar to the Chl-SST relationship shown in Fig. 1C. For instance, half of the area in the North Pacific where SST and Chl inversely evolve (yellow in Fig. 1C) shows parallel decreases in Chl and ZML (purple in Fig. 3B). The large areas of inverse Chl-SST in the equatorial and south Pacific are nearly absent from the Chl-ZML relationship. This shows that the Chl-ZML relationship probably bears the imprints of more-regional changes, intervening at shorter, interannual, scales.

Several studies have shown changes in global ocean phytoplankton over the past 10 years (*3*, *4*, *15*, *16*), and interpreting these changes as being indicative of long-term trends is tempting. Our results show that the multidecadal Chl changes observed over the CZCS-to-SeaWiFS era appear related to basin-scale oscillations in the physical environment (the PDO and AMO). These oscillations can alternately weaken or emphasize the possible effects of global warming (*17*), making difficult the identification of trends over short time series. In the Pacific, the PDO

results from the superposition of SST fluctuations forced in equal parts, at decadal time scales, by the variability of the Aleutian low, the El Niño–Southern Oscillation, and zonal advection anomalies in the Kuroshio-Oyashio Extension (*18*). In the Atlantic Ocean, the AMO has been linked to multidecadal variations in the strength of the meridional overturning circulation (*19*). Therefore, these processes all intervene to various degrees in shaping the global decadal-scale Chl variability, through their role on the overall stratification of the ocean, as revealed here through the

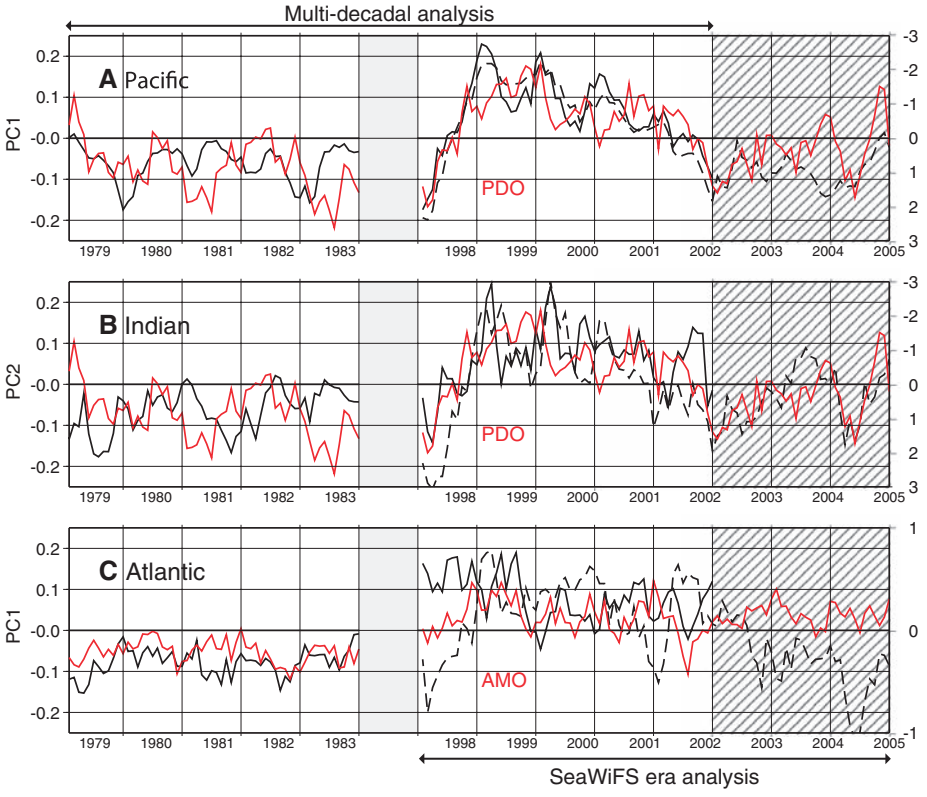

Fig. 2. The Chl-SST common time variability corresponding to the MEOF patterns (fig. S2) for the Pacific (**A**), Indian (**B**), and Atlantic (**C**) Oceans (black thick curve and scale on the left axes). PDO and AMO are superimposed as indicated (red curves and scales on the right axes). The Chl-SST common time variability issued from the MEOFs performed over the 1998–2005 era on the standard Chl SeaWiFS product (*8*) is shown as a dashed line on the right side of each panel. The diagonally hatched area sets the limit between the decadal analysis (using reanalyzed SeaWiFS data up to 2002 only) and the analysis presented in the supporting online material over the SeaWiFS era until 2005 (fig. S3).

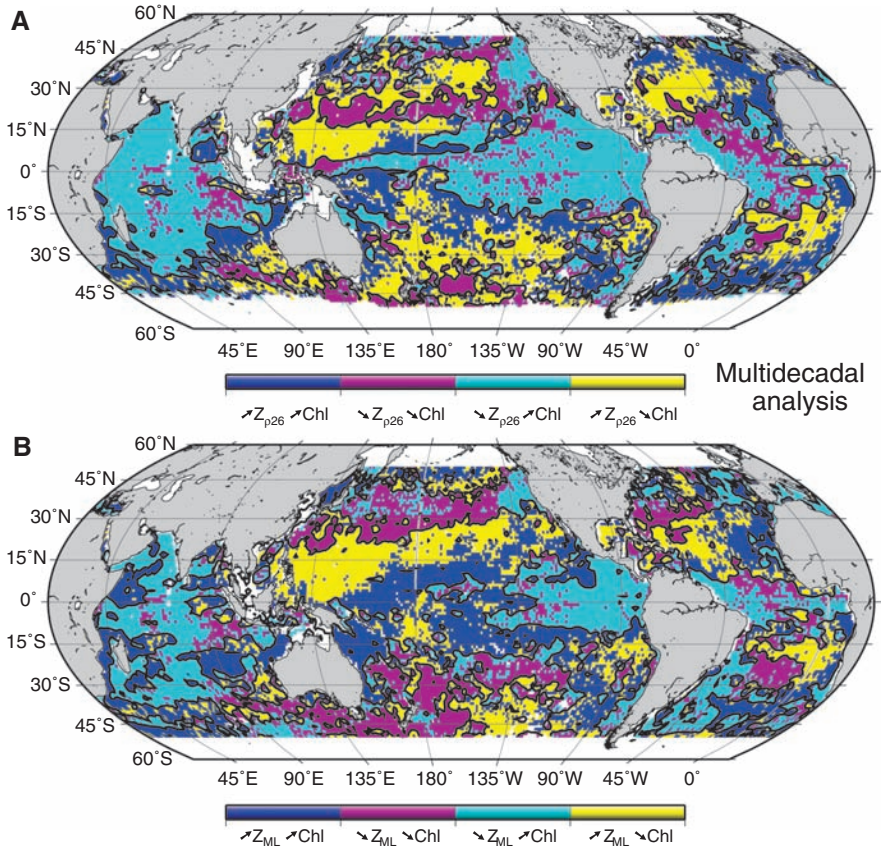

Fig. 3. Mapping of areas with concomitant parallel or opposite changes from 1979–1983 to 1998–2002 of Chl and $Z\rho_{26}$ (**A**), and of Chl and ZML (**B**), with $Z\rho_{\rho 26}$ and ZML determined from the SODA (*8*) data set. Dark blue and yellow correspond to deeper $Z\rho_{26}$ or ZML, whereas purple and light blue show areas of shallower $Z\rho_{26}$ or ZML.

Chl-$Z\rho_{26}$ and Chl-ZML relationships. This important role of ocean physics indicates that the observed Chl changes primarily reflect biomass changes due to dampened or increased nutrient fluxes to the upper lit layers. Changes in the photoacclimation state of phytoplankton probably also intervene, without obscuring the global picture, however. Quantifying the respective role of both phenomena would require the parallel examination of Chl and other quantities more directly tied to biomass.

A basin-specific response of phytoplankton to large-scale climate oscillators has been shown here. This result argues for a more accurate representation of decadal regimes into global ocean models, whose predictions of the response of ecosystems to global change are still uncertain (*20*–*22*). Such improvements are crucial for a better forecast of the impact of climate change on ecosystems and carbon fluxes. Our results also show that dampening the effect of interannual variability by averaging over two decades allows the decadal variability to be revealed and analyzed. Therefore, it can be anticipated that averaging over several decades may eventually reveal longer-term trends related to subtle changes in physical forcing. This emphasizes the critical importance of reanalyzing historical data sets (*23*, *24*) and of continuing the construction of climate-quality satellite data records in the next decades (*25*).

References and Notes

1. D. Antoine, A. Morel, H. R. Gordon, V. F. Banzon, R. H. Evans, *J. Geophys. Res.* **110**, C06009 (2005).
2. W. W. Gregg, M. E. Conkright, *Geophys. Res. Lett.* **29**, 1730 (2002).
3. C. R. McClain, S. R. Signorini, J. R. Christian, *Deep Sea Res. Part II Top. Stud. Oceanogr.* **51**, 281 (2004).
4. M. J. Behrenfeld *et al*., *Nature* **444**, 752 (2006).
5. J. A. Yoder, M. A. Kennelly, *Oceanography (Wash. D.C.)* **19**, 152 (2006).
6. C. R. McClain, G. C. Feldman, S. B. Hooker, *Deep Sea Res. Part II Top. Stud. Oceanogr.* **51**, 5 (2004).
7. W. A. Hovis *et al*., *Science* **210**, 60 (1980).
8. Materials and methods are available as supporting material on *Science* Online.
9. T. M. Smith, R. W. Reynolds, T. C. Peterson, J. Lawrimore, *J. Clim.* **21**, 2283 (2008).
10. N. J. Mantua, S. R. Hare, Y. Zhang, J. M. Wallace, R. C. Francis, *Bull. Am. Meteorol. Soc.* **78**, 1069 (1997).
11. D. Enfield, A. Mestas-Nunez, P. Trimble, *Geophys. Res. Lett.* **28**, 2077 (2001).
12. N. J. Mantua, S. R. Hare, *J. Oceanogr.* **58**, 35 (2002).
13. J. Hua, W. Dexing, W. Xiuquan, *Chin. J. Oceanol. Limnol.* **24**, 111 (2006).
14. J. A. Carton, B. S. Giese, *Mon. Weather Rev.* **136**, 2999 (2008).
15. S. C. Doney, *Nature* **444**, 695 (2006).
16. J. J. Polovina, E. A. Howell, M. Abecassis, *Geophys. Res. Lett.* **35**, L03618 (2008).
17. D. M. Smith *et al*., *Science* **317**, 796 (2007).
18. N. Schneider, B. D. Cornuelle, *J. Clim.* **18**, 4355 (2005).
19. J. R. Knight, R. J. Allan, C. K. Folland, M. Vellinga, M. E. Mann, *Geophys. Res. Lett.* **32**, L20708 (2005).
20. L. Bopp *et al*., *Global Biogeochem. Cycles* **15**, 81 (2001).
21. J. L. Sarmiento *et al*., *Global Biogeochem. Cycles* **18**, GB3003 (2004).
22. B. Schneider, *Biogeosciences* **5**, 597 (2008).
23. R. H. Evans, H. R. Gordon, *J. Geophys. Res.* **99**, 7293 (1994).
24. P. G. Falkowski, C. Wilson, *Nature* **358**, 741 (1992).
25. C. R. McClain, S. B. Hooker, G. C. Feldman, P. Bontempi, *Eos* **87**, 337 (2006).

26. We thank the Agence Nationale de la Recherche (Paris) for the financial support for this work carried out within the frame of the Globphy project, NASA (U.S.) for providing the SeaWiFS global chlorophyll data, and the U.S. National Oceanographic and Atmospheric Administration National Climatic Data Center for the ERSST v3 data set. We thank D. Siegel, H. Claustre, Y. Huot, and A. Morel for the comments they provided on early versions of the manuscript, and three anonymous reviewers for their comments and helpful suggestions.

Supporting Online Material

www.sciencemag.org/cgi/content/full/326/5957/1253/DC1
Materials and Methods
SOM Text
Figs. S1 to S3
References

29 May 2009; accepted 24 September 2009
10.1126/science.1177012

Global Signatures and Dynamical Origins of the Little Ice Age and Medieval Climate Anomaly

Michael E. Mann,[1]* Zhihua Zhang,[1] Scott Rutherford,[2] Raymond S. Bradley,[3] Malcolm K. Hughes,[4] Drew Shindell,[5] Caspar Ammann,[6] Greg Faluvegi,[5] Fenbiao Ni[4]

Global temperatures are known to have varied over the past 1500 years, but the spatial patterns have remained poorly defined. We used a global climate proxy network to reconstruct surface temperature patterns over this interval. The Medieval period is found to display warmth that matches or exceeds that of the past decade in some regions, but which falls well below recent levels globally. This period is marked by a tendency for La Niña–like conditions in the tropical Pacific. The coldest temperatures of the Little Ice Age are observed over the interval 1400 to 1700 C.E., with greatest cooling over the extratropical Northern Hemisphere continents. The patterns of temperature change imply dynamical responses of climate to natural radiative forcing changes involving El Niño and the North Atlantic Oscillation–Arctic Oscillation.

Considerable progress has been made over the past decade in using climate "proxy" data to reconstruct large-scale trends in past centuries, and in using climate models to assess the roles of natural and anthropogenic forcing in those trends (*1*). Owing in part to the sparseness of the available proxy data, less progress has been made in identifying the underlying spatial patterns of those changes, let alone the causal factors behind them. Yet a better understanding of past patterns of climate change and their causes (e.g., the role of past changes in the El Niño–Southern Oscillation, or ENSO) may be even more important for validating the regional-scale projections, which are paramount in assessing future climate change impacts.

Patterns of past climate change can be estimated through the simultaneous analysis of multiple spatially distributed proxy records. Such analyses have been performed via statistical reconstruction (*2*–*8*) and model assimilation approaches (*9*), but available proxy networks have been insufficient for estimating spatially resolved large-scale temperature reconstructions beyond the past few centuries (*2*, *4*, *7*).

Here, we employ a diverse multiproxy network previously used to estimate global and hemispheric mean annual temperature trends (*10*) to reconstruct global patterns of surface temperature changes over the past 1500 years. We use a climate field reconstruction (CFR) approach (*11*) that has been rigorously tested with synthetic "pseudoproxy" networks generated from forced climate model simulations (*12*). We interpret the resulting reconstructions in the context of results from climate model simulations forced by estimated past changes in natural (solar and volcanic) radiative forcing.

We employ the global proxy data set used by (*13*) comprising more than a thousand tree-ring, ice core, coral, sediment, and other assorted proxy records spanning the ocean and land regions of both hemispheres over the past 1500 years. The surface temperature field is reconstructed by calibrating the proxy network against the spatial information contained within the instrumental annual mean surface temperature field (*14*) over a modern period of overlap between proxy and instrumental data (1850 to 1995) using the RegEM CFR procedure (*12*) with additional minor modifications. Further details of

[1]Department of Meteorology and Earth and Environmental Systems Institute, Pennsylvania State University, University Park, PA 16802, USA. [2]Department of Environmental Science, Roger Williams University, Bristol, RI 02809, USA. [3]Department of Geosciences, University of Massachusetts, Amherst, MA 01003–9298, USA. [4]Laboratory of Tree-Ring Research, University of Arizona, Tucson, AZ 85721, USA. [5]NASA Goddard Institute for Space Studies, New York, NY 10025, USA. [6]Climate Global Dynamics Division, National Center for Atmospheric Research, Boulder, CO 80305, USA.

*To whom correspondence should be addressed. E-mail: mann@meteo.psu.edu